Electronic Supplementary Material (ESI) for Journal of Materials Chemistry A.
This journal is © The Royal Society of Chemistry 2017

Electronic Supplementary Information for

Thermocatalytic Syntheses of Highly Defective Hybrid Oxide Nano-catalysts for Photocatalytic Hydrogen evolution

Xiaole Weng,[a] Yili Zhang,[a] Feng Bi,[a] Fan Dong,[b] Zhongbiao Wu[a,*] and Jawwad A. Darr[c,*]

[a] Key Laboratory of Environment Remediation and Ecological Health, Ministry of Education, College of Natural Resources and Environmental Science, Zhejiang University, Zhejiang Provincial Engineering Research Center of Industrial Boiler & Furnace Flue Gas Pollution Control, 388 Yuhangtang Road, Hangzhou, 310058, P. R. China. Fax/Tel: 0086 571 8795308; E-mail: zbwu@zju.edu.cn.

[b] Chongqing Technology& Business University, College of Environmental& Biological Engineering, Chongqing, 400067, P. R. China.

[c] Department of Chemistry, University College London, Christopher Ingold Laboratories, 20 Gordon Street, London, WC1H 0AJ, UK.

***Corresponding Authors**

Prof. Zhongbiao Wu, E-mail: zbwu@zju.edu.cn;

Prof. Jawwad A. Darr, E-mail: j.a.darr@ucl.ac.uk.

Table S1 XRD Rietveld refinement result of sc-TiO_2 (S1) and sc-NiO-TiO_2-N_2 (S2)

	Lattice parameter						Structure				
	Crystal system	Space group	a	b	c	α=β=γ	Atoms	x	y	z	occupancy
S1	Tetragonal	I41/amd	3.7909(4)	3.7909(4)	9.507(2)	90	Ti	0	0.25	0.875	1
							O	0	0.25	0.0814	1
S2-1	Tetragonal	I41/amd	3.7875(3)	3.7875(3)	9.508(2)	90	Ti	0	0.25	0.875	1
							O	0	0.25	0.0814	0.84(1)
S2-2	Cubic	Fm-3m	4.1816(2)	4.1816(2)	4.1816(2)	90	Ni	0	0	0	1
							O	0.5	0.5	0.5	1

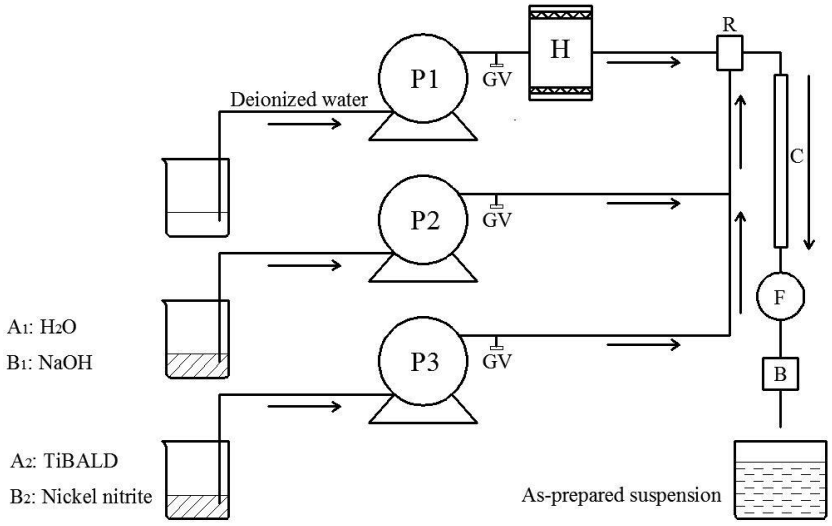

Fig. S1 Schematic diagram of continuous hydrothermal flow synthesis system (P, pump; GV, globe valve; H, heater; R, reactor; C, cooler; F, filter; B, back pressure valve).

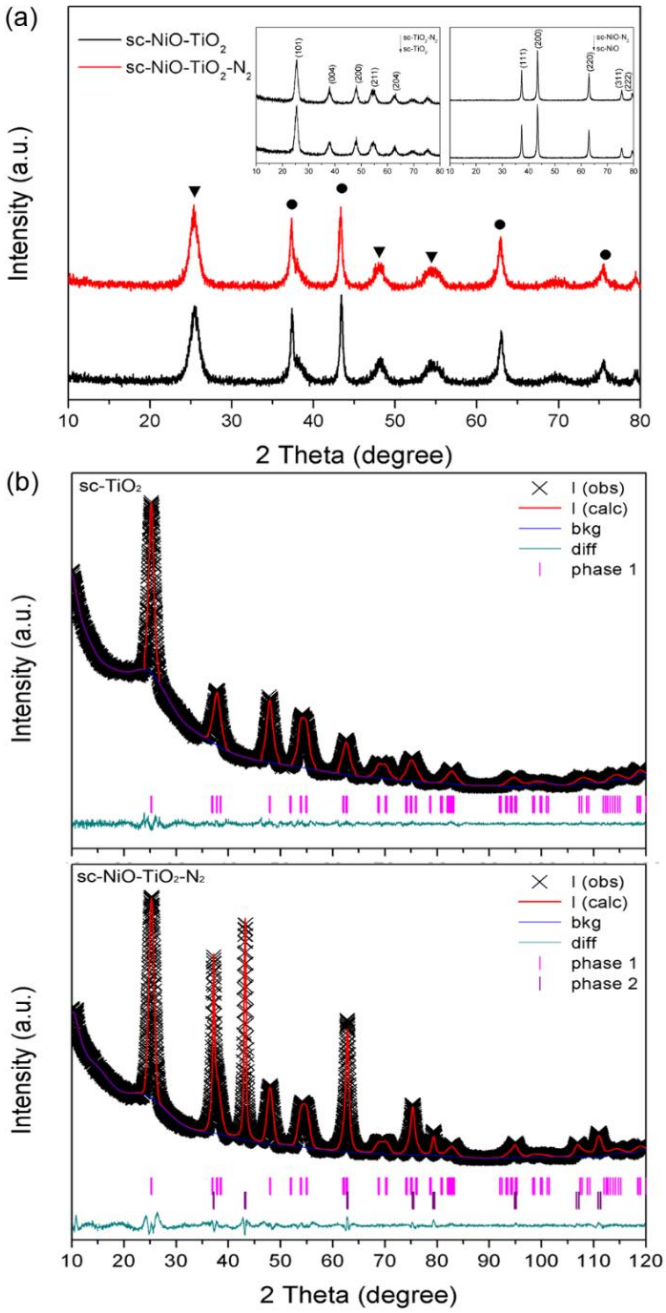

Fig. S2 (a) XRD patterns of sc-TiO_2, sc-TiO_2-N_2, sc-NiO, sc-NiO-N_2, sc-NiO-TiO_2, sc-NiO-TiO_2-N_2 and (b) XRD Rietveld refienment of sc-TiO_2 and sc-NiO-TiO_2-N_2 (I(obs): observed intensity; I(calc): calculated intensity; bkg: background; diff: diiference; ▼ (or phase 1): TiO_2; ● (or phase 2): NiO)

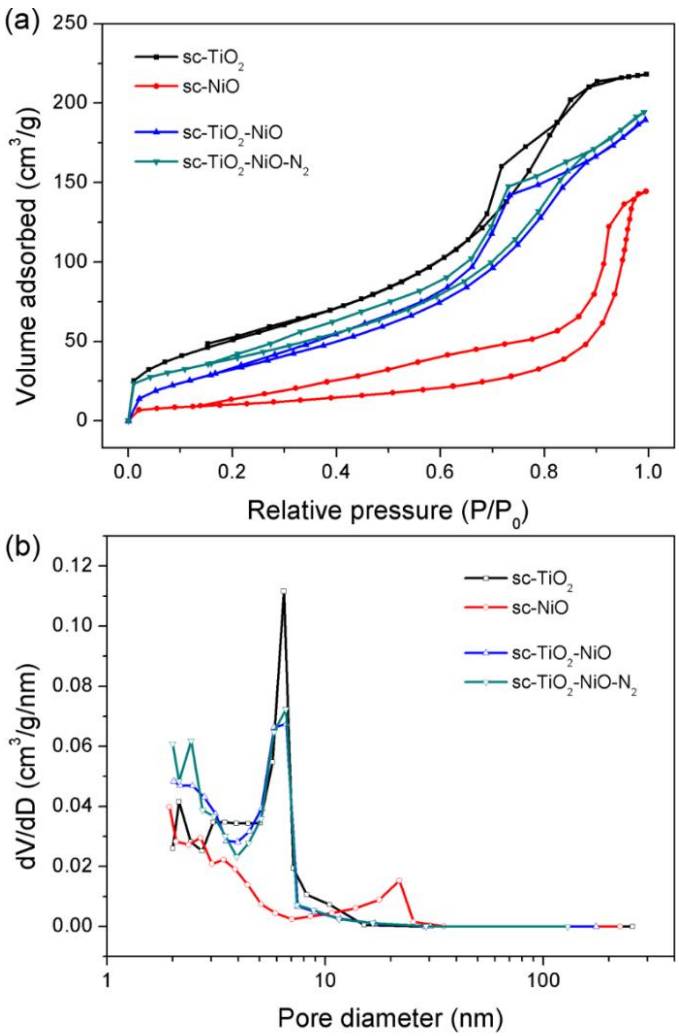

Fig. S3 (a) Adsroption isotherm and (b) pore size distribution of sc-TiO_2, sc-NiO, sc-NiO-TiO_2 and sc-NiO-TiO_2-N_2 samples.

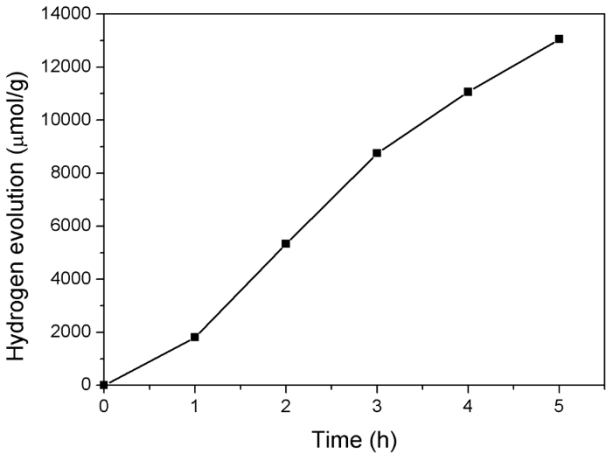

Fig. S4 Photocatalytic activities of 0.1wt% Pt doped sc-NiO-TiO_2-N_2 powders at room temperature.

Computational Methods

The reported calculation of energy band structure and density of states (DOS) of defect-free TiO_2 and defective TiO_2 were performed using a first-principle density functional theory (DFT).[1-3] The generalized gradient approximation proposed by Perdew, Burk and Ernzerhof (GGA-PBE) [4, 5] settled in CASTEP (Cambridge Serial Total Energy Package) was selected. To make the result more representative, defect-free and defective TiO_2 models for calculation were obtained from Crystallography Open Database. According to our XRD Rietveld refinement results (see **Table S1**), TiO_2 with COD ID of No. 9015929 [6] and No. 9008215 [7] were employed as the primitive cells for defect-free and defective TiO_2 calculation, respectively. A (2×3×1) supercell with 47 titanium atoms and 70 oxygen atoms ($Ti_{47}O_{70}$) were then built for the simulations of defect-free TiO_2 (see **Figure S5(a)**), while the supercell with 47 titanium atoms and 69, 67 and 60 oxygen atoms ($Ti_{47}O_{69}$, $Ti_{47}O_{67}$, $Ti_{47}O_{60}$) were built for defective TiO_2 (see **Fig. S5(b-d)**). In defective TiO_2, oxygen were mostly removed from the surface of the supercell, for oxygen vacancies in sc-NiO-TiO_2-N_2 catalysts mainly existed on the surface of TiO_2. Parameres during the simulation were set referred to the literature reported by Wu *et al*.[8] and our experimental results. The Tkatchenko-Scheffler method for DFT-D correction was used through out.[9]The energy cutoff was set at 400 eV, with the FFT grid of 48×48×48. The SCF tolerance and k-point were set as 10^{-6} eV/atom and 1×1×2, respectively. Moreover, a norm-conserving pseudopotential was chosen for its high accuracy.[10, 11]

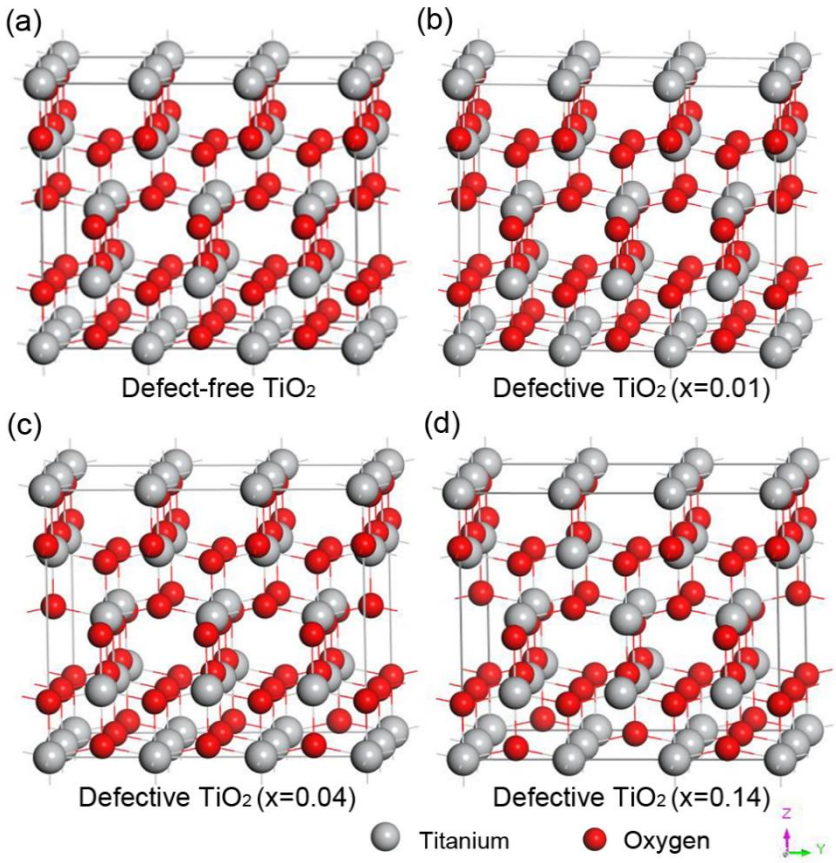

Fig. S5 Structure of (a) defect-free TiO_2 and (b-d) defective TiO_2 (x=0.01, 0.04 and 0.14) used for calculation of band structure and PDOS.

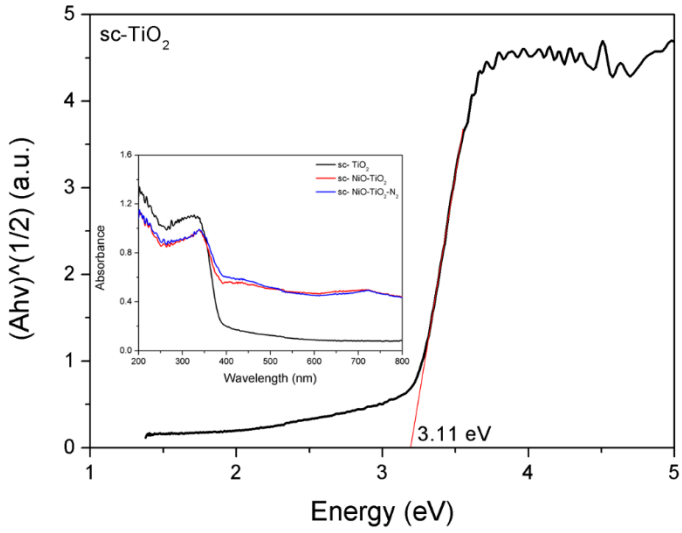

Fig. S6 UV-Vis spectra of sc-TiO_2, sc-NiO-TiO_2 and sc-NiO-TiO_2-N_2, and calculated band gap of defect-free sc-TiO_2.

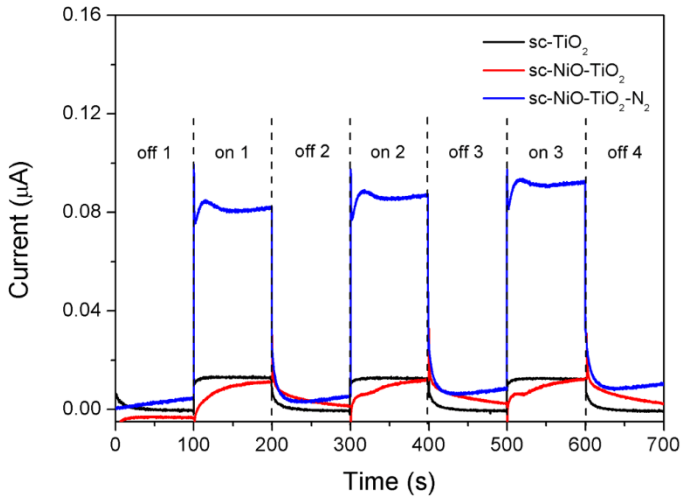

Fig S7. Transient photocurrents of sc-TiO_2, sc-NiO-TiO_2 and sc-NiO-TiO_2-N_2 under visible-light irradiation.

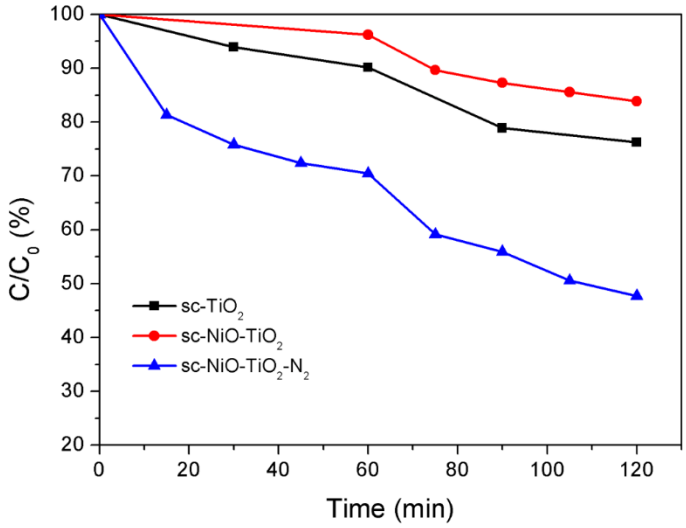

Fig. S8 Visible-light photocatalytic toluene oxidation activities of sc-TiO_2, sc-NiO-TiO_2 and sc-NiO-TiO_2-N_2.

XPS Analysis

Fig. S9(a) refers to Ni 2p spectra of NiO-TiO_2 (before and after N_2 treatment). Before heating, peaks at 853.5eV, 855.1 eV and 860.7 eV, assigned to the characteristic peaks of NiO, were clearly observed [12]. For NiO-TiO_2-N_2-300 °C hybrids, peaks at 853.2 eV, 854.9 eV and 860.2 eV belongning to Ni $2p_{3/2}$, and 870.6 eV、871.6 eV、878.7 eV for $Ni2p_{1/2}$ were surveyed. The energy differences between 853.2 eV (belongs to $Ni2p_{3/2}$) and 870.6 eV (belongs to $Ni2p_{1/2}$) was 17.4 eV, while that between 853.2 eV (belongs to $Ni2p_{3/2}$) and 871.6 eV (belongs to $Ni2p_{1/2}$) was 18.4 eV, indicating that trace NiO might be reduced and metallic Ni might form instead.[12-14] Compared with sc-NiO-TiO_2 mixtures, the sc-NiO-TiO_2-

N_2 hybrids shifted the Ni2p signal toward a lower value of binding energy for about 0.2 eV. This phenomenon was related to the augment of electron cloud density around Ni atoms, which was in accordance with the formation of metallic Ni.[15] The comparison of Ti2p of sc-NiO-TiO_2 and sc-NiO-TiO_2-N_2 is shown in **Fig. S9(b)**. The $Ti2p_{3/2}$ peak of sc-NiO-TiO_2-N_2 shifted from 458.9 eV to a lower binding energy compared to that of sc-NiO-TiO_2, indicating the fromation of Ti^{3+}.[16] **Fig. S9(c)** depicts the O 1s spectra of the samples. For pure TiO_2, only peaks at 530.0 eV and 531.4 eV, which were assigned to Ti-O lattice oxygen and -OH surface oxygen respectively, were surveyed.[17, 18] For sc-NiO-TiO_2 before N_2 treatment, peak at 529.3 eV in addition to the former ones was observed, which was ascribed to Ni-O lattice oxygen.[14] For sc-NiO-TiO_2-N_2 hybrids, C 1s signal of Ni-O lattice oxygen was observed at 528.7 eV, indicating that the density of electron cloud around Ni-O bend increased. C1s spectra of the samples was shown in **Fig. S9(d)**. Peaks at 284.8 eV was usually ascribed to adventitious carbon from the instrument, as well as the carbon residues from the incomplete oxidation of lactate species.[19, 20] Peaks at 286.3 eV and 288.6 eV were assigned to C-O and C=O respectively, demonstrating the coverage of carbonate on the surface of particles.[21] For sc-NiO-TiO_2-N_2 hybrids, the intensity of XPS signal at 288.7 eV was lower that that of TiO_2 and NiO-TiO_2, indicating that part of the surface carbonate released during the N_2 treatment process. According to ESR spectra, Ni2p spectra and O1s spectra, it can be conjectured that under the radiation of X-ray, free electrons located in the bulk of sc-NiO-TiO_2-N_2 moved to the surfacial Ti^{3+}, Ni^{2+} and oxygen vacancies, leading to the formation of the photocurrent.

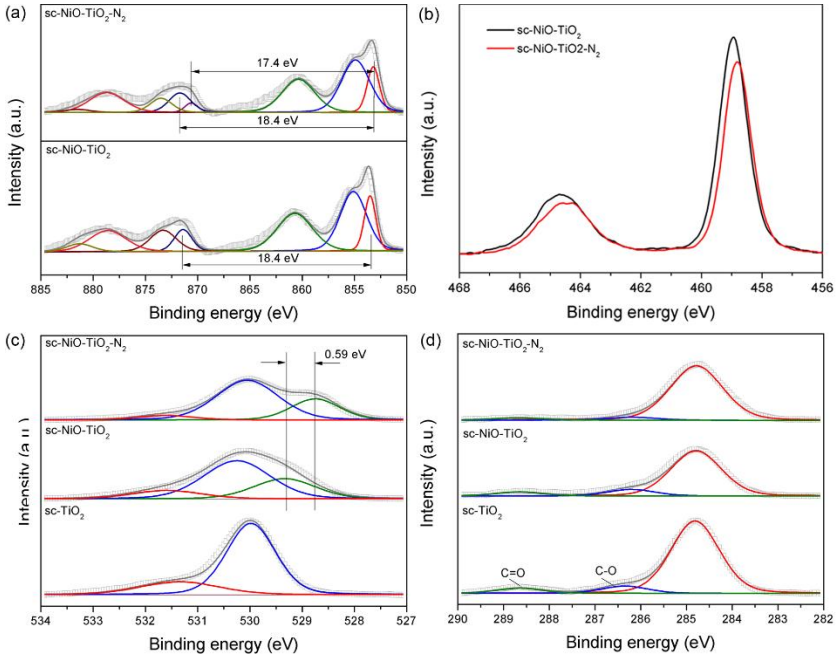

Fig. S9 XPS spectra of (a) Ni2p, (b) Ti2p, (c) O1s and (d) C1s of selected sc-TiO_2, sc-NiO-TiO_2 and sc-NiO-TiO_2-N_2 samples.

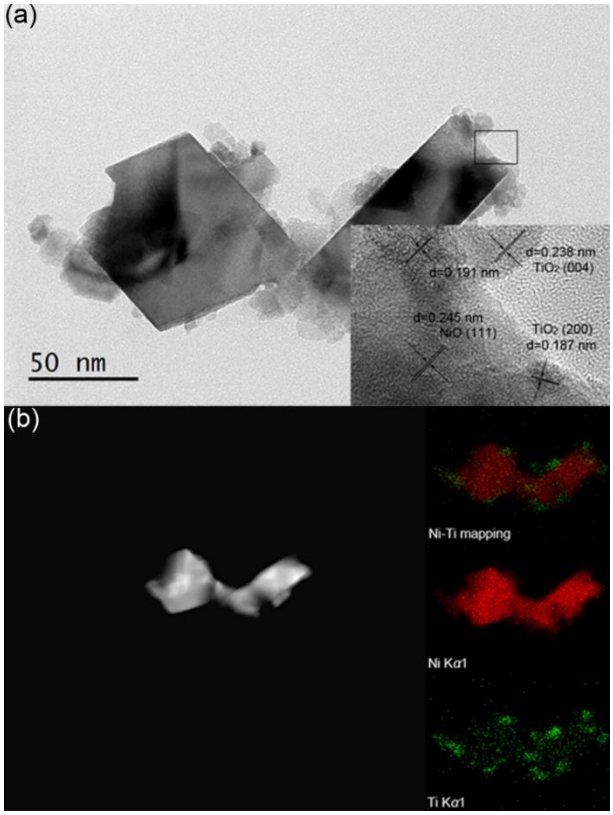

Fig. S10 (a) HR-TEM and (b) EDX-mapping of sc-NiO-TiO_2-N_2 sample.

References

1. M. D. Segall, P. J. D. Lindan, M. J. Probert, C. J. Pickard, P. J. Hasnip, S. J. Clark and M. C. Payne, *J. Phys. - Condens. Matter*, 2002, **14***,* 2717-2744.
2. N. Yang, Y. Liu, H. Wen, Z. Tang, H. Zhao, Y. Li, and D. Wang, *ACS Nano* 2013, **7***,* 1504-1512.
3. P. J. D. Lindan, N. M. Harrison, M. J. Gillan and J. A. White, *Phys. Rev. B* 1997, **55***,* 15919-15927.
4. J. P. Perdew, and W. Yue, *Phys. Rev. B*, 1986, **32***,* 8800-8802.
5. J. P. Perdew, K. Burke, M. Ernzerhof, *Phys. Rev. Lett.*, 1996, **77***,* 3865-3868.
6. C. J. Howard, T. M. Sabine, and F. Dickson, *Acta Cryst.,* 1991, **B47**, 462-468.
7. M. Horn, C. F. Schwerdtfeger and E. P. Meagher, *Z. Kristallorgr.* 1972, **136**, 273-281.
8. M. C. Wu, H. C. Liao, Y. C. Cho, G. Tóth, Y. F. Chen, W. F. Su and K. Kordás, *J. Mater. Chem. A*, 2013, **1***,* 5715-5720.
9. A. Tkatchenko and M. Scheffler, *Phys. Rev. Lett.*, 2009, **102***,* 073005.
10. L. Kleinman, *Phys. Rev. B*, 1980, **21**, 2630-2631.
11. C. Hartwigsen, S. Goedecker, and J. Hutter, *Phys. Rev. B* 1988, **58***,* 3641-3662.
12. H. W. Nesbitt, D. Legrand and G. M. Bancroftt, *Phys. Chem. Minerals* 2000, **27**, 357-366.
13. H. Shang, K. Pan, L. Zhang, B. Zhang, and X. Xiang, *Nanomaterials*, 2016, **6**, 103.
14. M. C. Biesinger, B. P. Payne, L. W. M. Lau, A. Gerson and R. S. C. Smart, *Surf. Interface Anal.*, 2009, **41**, 324-332.
15. D. Huang, L. Yin and J. Niu, *Environ. Sci. Technol.* 2016, **50**, 5857-5863.
16. M. Xing, W. Fang, M. Nasir, Y. Ma, J. Zhang and M. Anpo, *J. Catal.*, 2013, **297**, 236-243.
17. G. S. Herman, Z. Dohnalek, N. Ruzycki, and U. Diebold, *J. Phys. Chem. B* 2003, **107**, 2788-2795.
18. H. Choi and M. Kang, *Int. J. Hydrogen Energ.*, 2007, **32**, 3841-3848.
19. P. Wang, P. S. Yap and T. T. Lim, *Appl. Catal. A-Gen.*, 2011, **399**, 252-261.
20. J. Wang, D. N. Tafen, J. P. Lewis, Z. Hong, A. Manivannan, M. Zhi, M. Li, and N. Wu, *J. Am. Chem. Soc.*, 2009, **131**, 12290-11297.
21. B. Liu, L.M. Liu, X. F. Lang, H. Y. Wang, X. W. Lou and E. S. Aydil, *Energ. Environ. Sci.*, 2014, **7**, 2592-2597.